**Journal of Neonatal Surgery**
***ISSN(Online): 2226-0439***
***Vol. 14, Issue 32s (2025)***
*https://www.jneonatalsurg.com*

OPEN ACCESS

# Optimized Approach for Precise Segmentation of COVID-19 Infected Regions in Chest X-ray Images

**Parashuram Bannigidad[1], Vaishali Kale[2]**

[1]Professor, Department of Computer Science Rani Channamma University, Belagavi-591156, Karnataka, India.
Email ID: parashurambannigidad@gmail.com
[2]Research Scholar, Department of Computer Science Rani Channamma University, Belagavi-591156, Karnataka, India.
Email ID: vrajarani.rns@gmail.com

Cite this paper as: Parashuram Bannigidad, Vaishali Kale, (2025) Optimized Approach for Precise Segmentation of COVID-19 Infected Regions in Chest X-ray Images. *Journal of Neonatal Surgery*, 14 (32s), 476-485.

**ABSTRACT**
The swift and devastating impact of infectious diseases like COVID-19 has caused significant health and economic losses globally. Non-invasive methods, such as chest X-rays, are critical for COVID-19 detection, given the labor-intensive and time-consuming nature of PCR-based diagnosis. Advanced image processing techniques enhance chest X-ray analysis by improving image quality, extracting critical features, isolating lung regions, facilitating automated detection of infection patterns, and supporting radiologists in accurate diagnosis and disease monitoring. This paper introduces a hybrid methodology that leverages the UNet3+ model with a ResNet50 backbone for precise lung segmentation, ensuring enhanced focus and accuracy in subsequent analyses. The lung segmentation guides an iterative global thresholding (IGT)-based approach to detect COVID-19 infection patterns. Additionally, the methodology incorporates the Watershed algorithm as a post-processing step to refine the region of interest (ROI) boundaries, ensuring improved delineation of infection areas and reducing artifacts or noise. This integrated approach enhances the reliability and precision of automated COVID-19 diagnosis using chest X-rays. Experiments conducted on datasets from Lakeview Hospital, Goaves, Belagavi, and Kaggle validate the proposed method. Results show high performance metrics, including Accuracy (0.95), Precision (0.95), Recall (0.92), F1 Score (0.95), Dice Coefficient (0.97), Specificity (0.98), and Jaccard Index (0.96), with a mean squared error (MSE) of 0.1. The proposed method outperforms segmentation techniques like Adaptive Mean Thresholding, Otsu, Sauvola, and Niblack. Comparisons with manual results from medical experts and radiologists further confirm its effectiveness.

**Key Words:** *Computer vision in healthcare, Image processing, Segmentation, IGT, thresholding*

## 1. INTRODUCTION

Coronavirus is a disease that comes from Severe Acute Respiratory Syndrome (SARS) and Middle East Respiratory Syndrome (MERS). [1] A COVID-19 infection can cause serious problems such as acute kidney failure, septic shock, heart attack, and pulmonary edema. [2] In this context, timely identification becomes vital in ensuring patients receive appropriate care and avoid the further spread of the disease.[3] The predominant method for detecting COVID-19 is real-time polymerase chain reaction (RT-PCR), which is known for its elevated rate of inaccurate negative results and can require up to 48 hours for results. Its sensitivity typically falls between 70 to 90[4] . Chest X-rays and CT- scans are well-known radiographic techniques used for the identification and assessment of COVID-19. Each method has its own set of advantages and disadvantages. CT-scans require more expensive equipment compared to chest X-rays. Additionally, the disinfection process for CT- scans is longer than for chest X-rays. CT-scans expose patients to higher levels of ionizing radiation compared to chest X-rays. Overall, due to their availability and lower radiation exposure, chest X-rays are generally preferred over CT-scans in hospitals. [5] Several medical professionals and radiologists have acknowledged the efficacy of employing chest radiography for COVID-19 detection, highlighting its similar performance to the RT-PCR test and achieving a 90% accuracy rate. [6]

Diagnosing COVID-19 manually from large volumes of chest X-rays is both impractical and labour-intensive.[7] Therefore, automated and real-time analysis of radiographic images is essential to assist doctors in accurately detecting COVID-19 infections. Machine learning (ML) and deep learning (DL) methods, combined with image processing techniques, have become indispensable in medical imaging due to their ability to process vast datasets beyond human capabilities. These approaches not only reduce physicians' workload but also enhance diagnostic precision and statistical reliability [5]

Computer Vision (CV), which focuses on computational methods for interpreting visual data, has recently seen significant success in medical imaging, with segmentation emerging as a particularly effective strategy. [7] Studies have verified that segmentation plays a pivotal role in practical applications. [8] Image segmentation involves partitioning an input image into different segments with a strong correlation with the region of interest (RoI) in the given image. It aids in removing irrelevant background information, reducing the risk of data leakage, and directing the machine learning model's attention towards the most critical regions of an image. The primary goal of segmentation methods is to pinpoint areas in an image that demand closer inspection. Lung segmentation in X-rays, for instance, holds significance in diagnosing various diseases such as pneumonia, tuberculosis, cystic fibrosis, cancer, and COVID-19, among others.

Research on COVID-19 identification using chest X-rays suggests that considering the entire image may lead Machine Learning or Deep Learning models to utilize features beyond lung opacities, potentially from areas outside the lungs. In such scenarios, the model may not effectively learn to identify pneumonia or COVID-19 but instead, other unrelated features. The study highlights that no model can be considered reliable without lung segmentation, even if it demonstrates strong classification performance. Lung segmentation helps remove significant noise and background information, compelling the model to focus solely on data from the lung area, which is the desired information in this context. Consequently, classification performance in models using segmented X-ray images tends to be more realistic, resembling human performance, and more logically sound. [9]

This research paper aims to enhance the accuracy of COVID-19 disease assessment using chest X-ray images by leveraging the advanced UNet3+ model with a ResNet50 backbone for precise lung segmentation. The UNet3+ architecture, with its robust feature extraction capabilities and enhanced skip connections, ensures accurate delineation of lung regions, even in complex cases. This segmentation is further refined using an iterative global thresholding technique to detect COVID-19-specific opacities, followed by a Watershed-based post-processing step to enhance boundary delineation and eliminate artifacts, thereby improving the overall precision and reliability of the assessment. Various researchers have worked on the detection of COVID-19 using chest X-ray and CT- scan images. Daniel P. et al. [10] have worked on image segmentation using basic thresholding techniques. Geetha N. et al. [11]used a modified median filter for image enhancement and statistical range for edge enhancement for Prediction of Lung Diseases from X-rays. Teixeira et al.[9] have worked on semantic segmentation using a U-Net CNN architecture and have performed the classification using three CNN architectures (VGG, ResNet, and Inception). Gianluca Maguolo et al. [8] have evaluated different testing protocols used for automatic COVID-19 diagnosis from X-ray images. Apurv Vashisht and Shiv Kumar [12] have analyzed thresholding-based, clustering-based, and edge-based segmentation methods. Bannigidad P, and Gudada C [13] have proposed a novel approach for the restoration of degraded historical Kannada handwritten documents using a combination of special local and global binarization techniques. Otsu N. [14] designed a global thresholding technique that specifies a global value for all of the image's pixel intensities to distinguish them as background and foreground objects. Devi M. et al. [15] introduced iterative thresholding-based image segmentation using 2D improved Otsu algorithm. Wand D. et al. [16] have proposed an efficient iterative thresholding method for multi-phase image segmentation. This research paper aims to propose an innovative methodology that combines lung segmentation using the UNet3+ model with a ResNet50 backbone, integrated with an iterative global thresholding-based algorithm, and supplemented by a Watershed-based post-processing step for refining segmented regions in chest X-ray images. The adoption of UNet3+ enhances the segmentation accuracy with its advanced multi-scale feature extraction capabilities, leveraging deep skip pathways to improve the capture of fine details in complex images. The ResNet50 backbone makes a significant contribution by providing a powerful residual network structure that mitigates the vanishing gradient problem, thereby enabling more effective learning of deeper features. This hybrid approach is specifically designed for the identification of COVID-19, providing a robust and precise method for accurately segmenting the affected areas, ensuring high performance even in challenging imaging conditions.

## 2. MATERIALS AND METHODS

The images used in this implementation were sourced from two distinct datasets: one from Lakeview Hospital, Goaves, Belagavi, and the other from the publicly available Kaggle website. The images are in '.png' format, and for consistency, all X-ray images were resized to 256x256 pixels. The implementation was carried out on a Windows system equipped with an 11th Gen Intel(R) Core (TM) i5-1135G7 processor and 8.00 GB of RAM. Image segmentation was executed using the Python programming language (version 3.9) within the Anaconda environment, utilizing Jupyter Notebook for development and execution.

## 3. PROPOSED METHOD

This research focuses on enhancing the accuracy of segmenting COVID-19 lesions in chest X-ray images to support medical professionals in diagnosis and analysis. The proposed methodology integrates lung segmentation using the UNet3+ model with a ResNet50 backbone, along with an Iterative Global Thresholding (IGT) algorithm, followed by a Watershed-based post-processing step for further refinement of the segmented regions. The UNet3+ model with a ResNet50 backbone first

isolates the lung regions, reducing the influence of irrelevant structures and ensuring that subsequent analysis is concentrated on areas most likely to exhibit disease-related patterns. The IGT algorithm is then applied within the segmented lung regions to enhance contrast and visibility of COVID-19-related abnormalities, while the Watershed algorithm refines the segmented regions, ensuring more precise delineation of infection patterns.

This combined approach offers several key advantages: it improves the visibility of opacities and abnormalities associated with COVID-19 by enhancing contrast, reduces noise and irrelevant artifacts in the image, and focuses the analysis on regions of interest. The inclusion of the Watershed-based post-processing step further ensures the segmentation's precision, allowing opacities and lesions indicative of COVID-19 to be distinctly identified and isolated. By leveraging the strengths of deep learning, traditional image processing techniques, and post-processing refinements, this method significantly enhances the accuracy and efficiency of COVID-19 detection in chest X-ray images, thereby aiding radiologists and clinicians in their diagnostic workflows.

The quality of the segmented images using IGT and the Watershed algorithm is compared to the ground truth annotations from medical experts and radiologists. The results are then compared with other segmentation techniques in the literature. Performance is measured using various metrics, including accuracy, precision, recall, F1 score, mean squared error (MSE), Dice coefficient, specificity, and Jaccard index, as explained below.

**a) Accuracy**

Accuracy measures the overall correctness of the segmentation, considering both the correctly segmented infected and non-infected regions.

Accuracy = (TP + TN) / (TP + TN + FP + FN) ---------- (1)

**b) Precision**

Precision evaluates how many of the predicted positive pixels (infected regions) are actually correct.

Precision = TP / (TP + FP) ----------(2)

**c) Recall (Sensitivity)**

Recall measures how many of the actual positive pixels (infected regions) are correctly identified by the model.

Recall = TP / (TP + FN) ---------- (3)

**d) F1 Score**

The F1 Score is the harmonic mean of precision and recall, balancing both metrics. It is particularly useful for imbalanced datasets.

F1 Score = 2 * (Precision * Recall) / (Precision + Recall) --------- (4)

**e) Mean Squared Error (MSE)**

MSE calculates the average squared difference between predicted and ground truth pixel values.

$MSE = (1/N) * \Sigma (\hat{y}_i - y_i)^2$ ----------(5)

**f) Dice Coefficient**

The Dice Coefficient quantifies the overlap between the predicted and ground truth regions.

Dice = (2 * TP) / (2 * TP + FP + FN) ---------- (6)

**g) Specificity**

Specificity measures how well the model identifies negative pixels (non-infected regions).

Specificity = TN / (TN + FP) ---------- (7)

**h) Jaccard Index (Intersection over Union, IoU)**

The Jaccard Index, specified in equation (1), measures the overlap between predicted and ground truth regions relative to their union.

Jaccard Index = TP / (TP + FP + FN) ----------(8)

For all the above evaluation measures, the proposed method gives better results as compared to other thresholding algorithms in the literature. The process is discussed below.

Thresholding is a technique used in image processing to create a binary image from a grayscale image by assigning a specific value (the threshold) to each pixel. Pixels with intensity values below the threshold are set to 0 (black), while pixels with

intensity values equal to or above the threshold are set to 1 (white).

The basic formula for thresholding is:

$$\text{Output Image}(x,y) = \begin{cases} 1, & \text{if Input Image } (x,y) \geq \text{ Threshold} \\ 0, & \text{otherwise} \end{cases} \text{ ----------(9)}$$

where:

- Output Image (x, y) is the value of the pixel at position (x, y) in the binary output image.
- Input Image (x, y) is the intensity value of the pixel at position (x, y) in the input grayscale image.
- Threshold is the threshold value used to convert the input image to a binary image.
- x and y are the spatial coordinates of a pixel in the image.
- The output image is binary, with pixel values of 0 (black) or 1 (white).

The proposed method is represented in the form of a flow diagram, which is shown in the Fig. 1

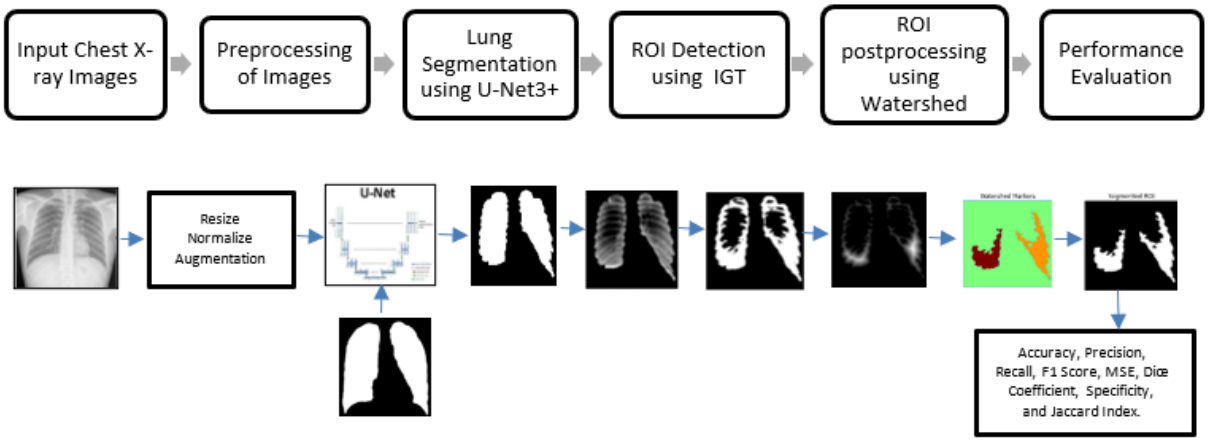


**Fig. 1. The flow diagram of the proposed method.**

The step-by-step algorithm for the proposed method is explained below

**Algorithm**

**Step 1. Preprocessing:**

1.1. Read the chest X-ray image and the corresponding ground truth segmentation mask.

1.2. Convert the image to grayscale.

1.3. Apply preprocessing steps, such as Adaptive histogram equalization for contrast enhancement, Gaussian blur to reduce noise, Resizing to a fixed size (e.g., 256x256), normalizing pixel values to the range [0, 1], Data Augmentation using random rotations, flips, and intensity shifts during training to increase model robustness

Step 2. **Lung Segmentation using U-Net**

2.1. Train the U-Net3+ model with a ResNet50 backbone using pre-processed images and masks, optimizing with binary cross-entropy loss and the Adam optimizer.

2.2. Use the binary masks generated by the U-Net3+ model to predict the lung masks from the input chest X-ray images.

2.3. Extract the lung regions by performing element-wise multiplication of the binary mask with the X-ray image.

**Step 3. Initialization:**

3.1. Convert the segmented lung image to a NumPy array.

3.2. Calculate the mean intensity value of all pixels within the segmented lung region to initialize the threshold $T_0$.

3.3. Set a maximum number of iterations *max_iterations*.

3.4. Set a threshold update tolerance $\epsilon$.

Step 4. **Apply Iterative Thresholding** only within the segmented lung regions to detect COVID-19-specific opacities or

abnormalities.

4.1. For each iteration *i* from 1 to *max_iterations*:

4.1.1. Calculate the mean intensity of the pixels below the threshold:

$$\mu_1 = \frac{1}{N_1} \sum_{x,y|I(x,y)<T_{i-1}} I(x,y)$$

4.1.2. Calculate the mean intensity of the pixels above the threshold:

$$\mu_2 = \frac{1}{N_2} \sum_{x,y|I(x,y)\geq T_{i-1}} I(x,y)$$

4.1.3. Calculate the new threshold value: $T_i = \frac{\mu_1+\mu_2}{2}$

4.1.4. Check the convergence criteria: $|T_i - T_{i-1}| < \epsilon$

4.1.5. If the convergence criteria are met, exit the loop.

**Step 5. Post-Processing:**

5.1. Use the Watershed algorithm as a post-processing step to refine the detected ROIs and enhance the delineation of boundaries, eliminating small artifacts and improving segmentation accuracy.

**Step 6. Extract the Performance Evaluation Measures:**

6.1. Compute TP, FP, TN, and FN based on the segmented and ground truth masks.

6.2. Compute Accuracy, Precision, Recall, F1 Score, MSE, Dice Coefficient, Specificity, and Jaccard Index.

**Step 7. Output:**

7.1. Return the segmented ROI from the X-ray image and the computed performance evaluation metrics specific to COVID-19 detection using X-ray images.

**Step 8. End Procedure**

**Mathematical Analysis:**

**i. Threshold Calculation**:

The threshold Ti for the i-th iteration is calculated as the sum of pixel values at each pixel position (row, column) (row α, column β) in the image as specified in equation 2:

$$T_i = \sum_{\alpha=1}^{M} \sum_{\beta=1}^{N} I_i(\alpha,\beta) \text{---------- (10)}$$

Here, M and N are the height and width of the image, Ii(α, β) is the pixel value at position (α,β) in the i-th iteration.

**ii. Pixel Value Adjustment :**

For each pixel (x,y) in the image, the average pixel value (Ti+1) calculated in the previous step is subtracted from the pixel value in the current iteration Ii(x,y)):

$$Is(x,y)=Ii(x,y)-Ti+1 \text{ ---------- (11)}$$

This step is used to normalize or adjust the pixel values based on the calculated threshold.

## 4. EXPERIMENTAL RESULTS AND DISCUSSION

To execute the implementation, the images have been collected from five distinct datasets. Two of the five datasets are collected from Lakeview Hospital, Goaves, Belagavi, and the remaining 3 datasets are from the Kaggle website which is freely available. The images are in the '.png' format. The implementation is done on the Windows system containing the 11th Gen Intel(R) Core(TM) i5-1135G7 processor and 8.00 GB RAM. Python programming language (3.9), in Anaconda, Jupyter Notebook environment is employed to perform image segmentation techniques.

For precise segmentation of lung regions in chest X-ray images, we employed the UNet3+ architecture with a ResNet50 backbone, an advanced variation of the standard U-Net model that significantly enhances segmentation performance. UNet3+ offers a more efficient hierarchical feature extraction process through its nested skip pathways and multiple encoders, ensuring better preservation of spatial information and stronger contextual understanding. Unlike traditional U-Net, which uses a simple encoder-decoder structure, UNet3+ incorporates deep supervision and additional skip connections, enhancing

feature propagation and improving segmentation accuracy, particularly in complex medical imaging tasks such as lung segmentation.

The encoder is powered by a ResNet50 backbone, which contributes deep feature extraction with residual learning. ResNet50's skip connections help to mitigate vanishing gradient problems, enabling the network to effectively learn more complex and deeper feature representations. The model's decoder, designed to reconstruct high-resolution segmentation maps, incorporates transposed convolutions that restore the image to the required size while benefiting from the enhanced feature maps extracted by the ResNet50 backbone.

The input chest X-ray images were resized to 256x256 pixels to match the model's input size requirements. The output was a binary mask highlighting the lung regions, where pixel values of 1 represented the lungs, and 0 represented the background. Post-processing techniques, such as morphological operations, were applied to refine the mask and eliminate small artifacts. This segmentation process provided accurate isolation of lung regions, forming a foundational step for downstream tasks like infection localization and quantification.

A block diagram of the UNet3+ architecture with ResNet50 backbone is shown in Fig. 2

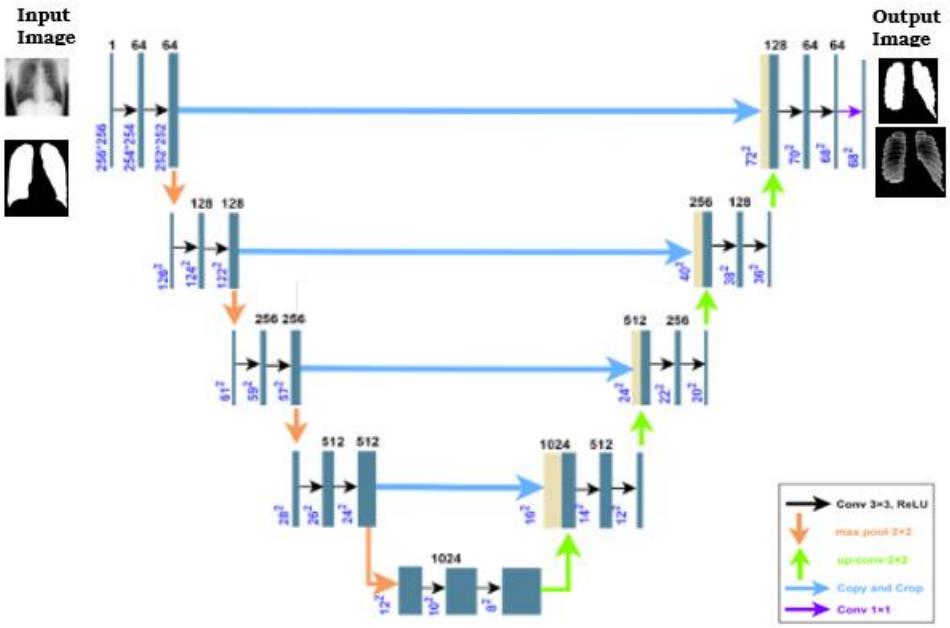


**Fig. 2. The block diagram of the UNet3+ architecture with ResNet50 backbone**

The network operates on grayscale input images resized to a resolution of 256x256 and outputs segmentation maps at 68x68 resolution. Feature extraction is achieved through convolutional layers with ReLU activations, and spatial dimensionality is reduced via 2x2 max-pooling operations. The ResNet50 backbone maximizes feature representation and minimizes spatial dimensions through downsampling at the bottleneck of the architecture. To mitigate overfitting, dropout layers are strategically integrated during training. In the subsequent upsampling phase, spatial dimensions are reconstructed, and skip connections from both shallow and deep layers of the encoder are integrated, ensuring better feature fusion and the preservation of fine-grained details. The network concludes with a 1x1 convolutional layer employing a sigmoid activation function to produce a pixel-wise binary classification mask. Model training is optimized using the binary cross-entropy loss function coupled with the Adam optimizer, ensuring effective convergence and robust segmentation performance.

The original image is obtained from the publicly available chest X-ray dataset on Kaggle website. Fig. 3. (a) shows original image converted to grey scale image. Fig. 3. (b) shows ground truth image. Fig. 3. (c) Segmented lung mask generated using U-Net architecture. Fig. 3. (d) Segmented lung image using U-Net3+ Fig. 3. (e) ROI Segmentation using IGT Fig. 3. (f) Segmented ROI using the proposed Method.

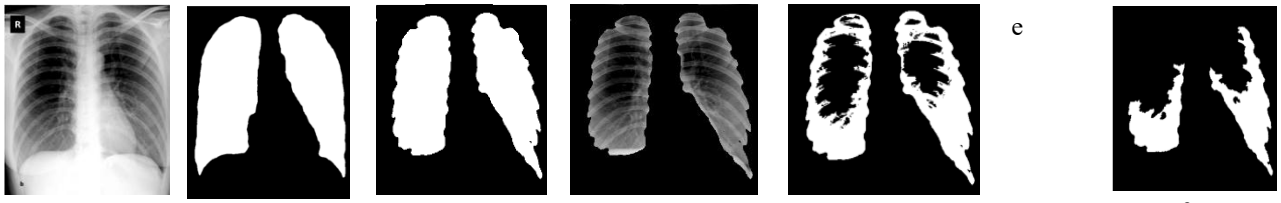


**Fig. 3. a. Original chest X-ray image b. Ground Truth Image c. Segmented lung mask generated using U-Net architecture d. Segmented lung image using U-Net3+ e. Segmented ROI using IGT f. Segmented ROI using the proposed Method.**

The performance measure values viz. Accuracy, Precision, Recall, F1 Score, MSE, Dice_Coefficient, Specificity and Jaccard_Indexare are obtained from Lakeview and Kaggle Datasets and the results are shown in Table 1.

| **Standard Datasets** | **Performance Evaluation** | **Segmentation techniques used by various researchers in the literature** | | | | **Proposed Method** |
|---|---|---|---|---|---|---|
| | | **Adaptive Mean Thresholding** | **Otsu** | **Sauvola** | **NiBlack** | |
| **Average of LakeView Datasets** | **Accuracy** | 0.90 | 0.91 | 0.89 | 0.88 | **0.96** |
| | **Precision** | 0.87 | 0.85 | 0.86 | 0.85 | **0.93** |
| | **Recall** | 0.85 | 0.87 | 0.85 | 0.84 | **0.91** |
| | **F1 Score** | 0.90 | 0.92 | 0.86 | 0.88 | **0.94** |
| | **MSE** | 0.13 | 0.12 | 0.13 | 0.13 | **0.10** |
| | **Dice_Coefficient** | 0.95 | 0.95 | 0.94 | 0.94 | **0.97** |
| | **Specificity** | 0.96 | 0.96 | 0.95 | 0.95 | **0.99** |
| | **Jaccard_Index** | 0.93 | 0.93 | 0.93 | 0.93 | **0.96** |
| **Average of Kaggle Datasets** | **Accuracy** | 0.88 | 0.91 | 0.87 | 0.87 | **0.95** |
| | **Precision** | 0.91 | 0.94 | 0.88 | 0.88 | **0.97** |
| | **Recall** | 0.87 | 0.89 | 0.86 | 0.86 | **0.92** |
| | **F1 Score** | 0.91 | 0.93 | 0.88 | 0.88 | **0.97** |
| | **MSE** | 0.14 | 0.12 | 0.14 | 0.14 | **0.11** |
| | **Dice_Coefficient** | 0.93 | 0.93 | 0.92 | 0.92 | **0.96** |
| | **Specificity** | 0.94 | 0.95 | 0.94 | 0.94 | **0.97** |
| | **Jaccard_Index** | 0.92 | 0.92 | 0.91 | 0.91 | **0.95** |

**Table 1 : Comparison of the experimental results with other techniques**

For Lakeview dataset, the values of Accuracy, Precision, Recall, F1 Score, MSE, Dice_Coefficient, Specificity and Jaccard_Indexare are 0.96, 0.93, 0.91, 0.94, 0.10, 0.97, 0.99, and 0.96 respectively and for the Kaggle dataset, the values of Accuracy, Precision, Recall, F1 Score, MSE, Dice_Coefficient, Specificity and Jaccard_Indexare are 0.95, 0.97, 0.92, 0.97, 0.11, 0.96, 0.97, and 0.95

The sample results of the proposed enhancement techniques are graphically presented in Fig. 4

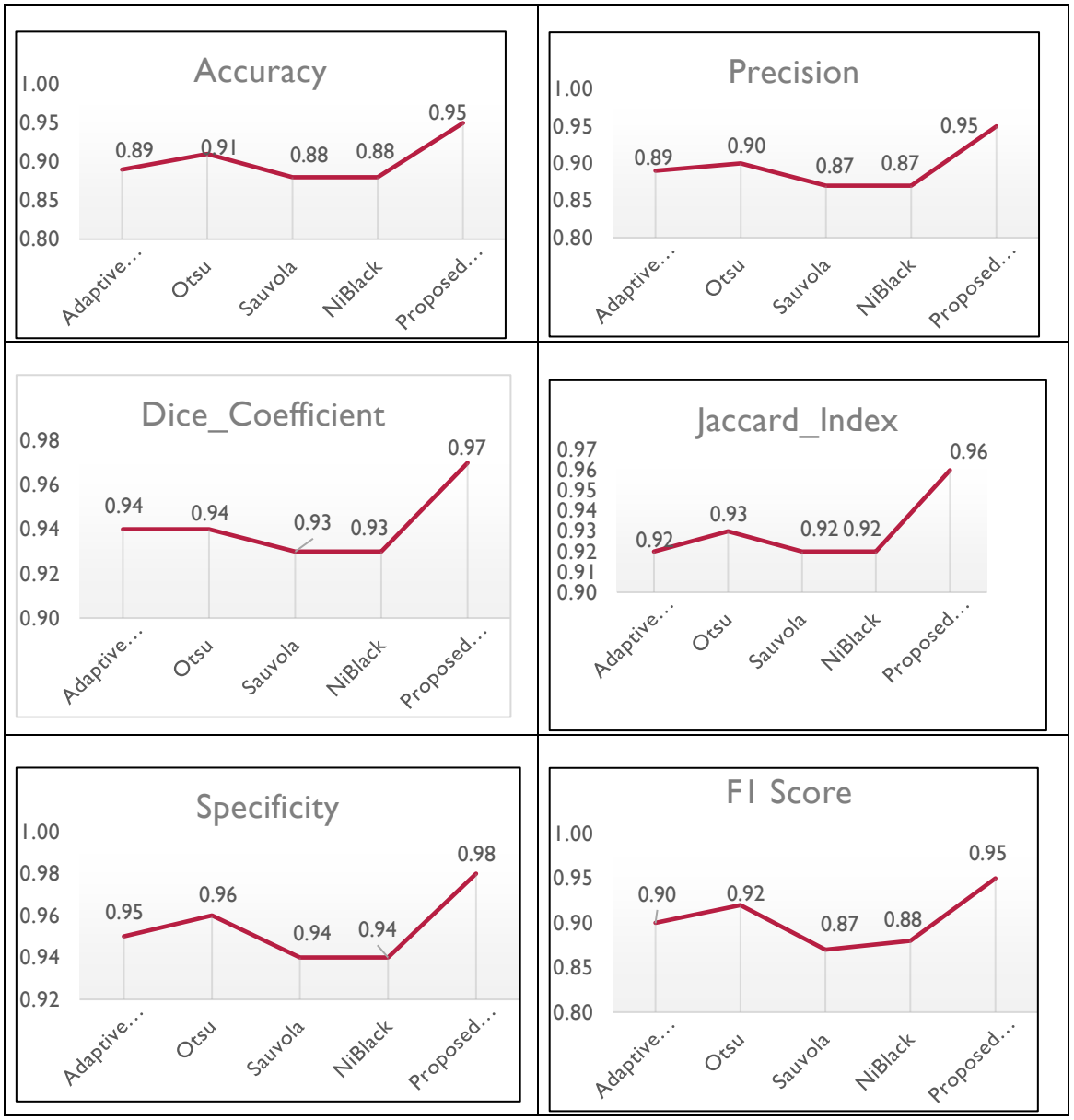

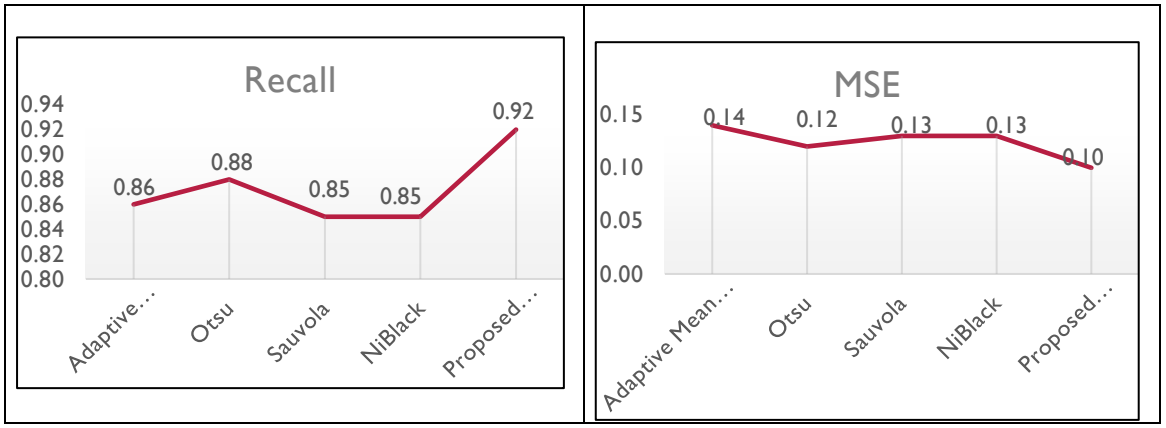


**Fig. 4. The sample results of the proposed segmentation technique.**

The proposed hybrid approach, which integrates lung segmentation using the UNet3+ model with a ResNet50 backbone and an iterative global thresholding (IGT) technique, followed by a Watershed-based post-processing step for refinement, demonstrated superior performance compared to existing segmentation methods in the literature. The IGT technique effectively segments the infected regions in X-ray images, while the Watershed algorithm further enhances the precision of the region boundaries. The results show that the proposed method achieves higher values for Accuracy, Precision, Recall, F1 Score, Dice Coefficient, Specificity, and Jaccard Index, while maintaining lower values for MSE, indicating its effectiveness in accurately identifying and segmenting COVID-19 affected regions. Thus, it can be concluded that this hybrid approach, with its combination of UNet3+, ResNet50, IGT, and Watershed refinement, outperforms other segmentation techniques reported in the literature.

## 5. CONCLUSION

This study aims to enhance the assessment of COVID-19 disease using chest X-ray images by employing a hybrid approach that integrates lung segmentation through the UNet3+ model with a ResNet50 backbone and Iterative Global Thresholding (IGT) to effectively isolate the infected areas. To refine the segmentation results, a Watershed-based post-processing step is applied, further improving the accuracy of the region of interest (ROI) delineation. The experimental results demonstrate that the average values of Accuracy, Precision, Recall, F1 Score, Dice Coefficient, Specificity, and Jaccard Index are 0.95, 0.95, 0.92, 0.95, 0.97, 0.98, and 0.96, respectively, with an MSE of 0.1. These values indicate that the proposed method outperforms other segmentation techniques, including Adaptive Mean Thresholding, Otsu, Sauvola, and Niblack, as highlighted in the literature. Furthermore, the results were compared with manual segmentation performed by radiologists, providing additional validation for the effectiveness of the proposed method. The algorithm was tested using datasets from Lakeview Hospital, Goaves, Belagavi, and the Kaggle website.

## ACKNOWLEDGEMENT

The authors express gratitude to Lakeview Hospital in Belagavi for providing X-ray images of COVID-19 patients. They also appreciate the valuable insights provided by Dr. Soumya P, a Radiologist, regarding COVID-19 identification. The authors are thankful to the Kaggle dataset, which is freely available to the public.

## REFERENCES

[1] W. Zhang, “Imaging changes of severe COVID-19 pneumonia in advanced stage,” Intensive Care Med, vol. 46, no. 5, pp. 841–843, May 2020, doi: 10.1007/S00134-020-05990-Y/FIGURES/1.

[2] S. Chavez, B. Long, A. Koyfman, and S. Y. Liang, “Coronavirus Disease (COVID-19): A primer for emergency physicians,” Am J Emerg Med, vol. 44, pp. 220–229, Jun. 2021, doi: 10.1016/J.AJEM.2020.03.036.

[3] A. S. Al-Waisy et al., “COVID-DeepNet: Hybrid Multimodal Deep Learning System for Improving COVID-19 Pneumonia Detection in Chest X-ray Images,” Computers, Materials & Continua, vol. 67, no. 2, pp. 2409–2429, Feb. 2021, doi: 10.32604/CMC.2021.012955.

[4] T. Asai, “COVID-19: accurate interpretation of diagnostic tests—a statistical point of view,” J Anesth, vol. 35, no. 3, p. 328, Jun. 2021, doi: 10.1007/S00540-020-02875-8.

[5] A. Narin, C. Kaya, and Z. Pamuk, "Automatic Detection of Coronavirus Disease (COVID-19) Using X-ray Images and Deep Convolutional Neural Networks," Pattern Analysis and Applications 2021 24:3, vol. 24, no. 3, pp. 1207–1220, Mar. 2020, doi: 10.1007/s10044-021-00984-y.

[6] A. Dangis et al., "Accuracy and reproducibility of low-dose submillisievert chest ct for the diagnosis of covid-19," Radiol Cardiothorac Imaging, vol. 2, no. 2, Apr. 2020, doi: 10.1148/RYCT.2020200196/ASSET/IMAGES/LARGE/RYCT.2020200196.FIG4.JPEG.

[7] G. Gaál, B. Maga, and A. Lukács, "Attention U-Net Based Adversarial Architectures for Chest X-ray Lung Segmentation," CEUR Workshop Proc, vol. 2692, Mar. 2020, Accessed: Mar. 25, 2024. [Online]. Available: https://arxiv.org/abs/2003.10304v1

[8] G. Maguolo and L. Nanni, "A critic evaluation of methods for COVID-19 automatic detection from X-ray images," Inf Fusion, vol. 76, pp. 1–7, Dec. 2021, doi: 10.1016/J.INFFUS.2021.04.008.

[9] L. O. Teixeira et al., "Impact of Lung Segmentation on the Diagnosis and Explanation of COVID-19 in Chest X-ray Images," Sensors 2021, Vol. 21, Page 7116, vol. 21, no. 21, p. 7116, Oct. 2021, doi: 10.3390/S21217116.

[10] P. Daniel, R. Raju, and G. Neelima, "Image Segmentation by using Histogram Thresholding".

[11] N. Geetha and S. J. S. A. Joseph, "Deep Separable Convolution Network for Prediction of Lung Diseases from X-rays," International Journal of Advanced Computer Science and Applications, vol. 13, no. 6, pp. 509–518, 2022, doi: 10.14569/IJACSA.2022.0130662.

[12] "Analysis of Image Segmentation Techniques: A Survey", Accessed: Mar. 26, 2024. [Online]. Available: www.erpublication.org

[13] P. Bannigidad and C. Gudada, "Restoration of degraded Kannada handwritten paper inscriptions (Hastaprati) using image enhancement techniques," 2017 International Conference on Computer Communication and Informatics, ICCCI 2017, Nov. 2017, doi: 10.1109/ICCCI.2017.8117697.

[14] N. Otsu, "THRESHOLD SELECTION METHOD FROM GRAY-LEVEL HISTOGRAMS.," IEEE Trans Syst Man Cybern, vol. SMC-9, no. 1, pp. 62–66, 1979, doi: 10.1109/TSMC.1979.4310076.

[15] M. P. A. Devi, T. Latha, and C. H. Sulochana, "Iterative thresholding based image segmentation using 2D improved Otsu algorithm," Global Conference on Communication Technologies, GCCT 2015, pp. 145–149, Nov. 2015, doi: 10.1109/GCCT.2015.7342641.

[16] D. Wang, H. Li, X. Wei, and X. P. Wang, "An efficient iterative thresholding method for image segmentation," J Comput Phys, vol. 350, pp. 657–667, Dec. 2017, doi: 10.1016/J.JCP.2017.08.020.